ChemComm

COMMUNICATION

View Article Online
View Journal | View Issue

A family of oxide–carbide–carbon and oxide–nitride–carbon nanocomposites†

Cite this: *Chem. Commun.*, 2014, 50, 5364

Received 30th September 2013,
Accepted 25th November 2013

DOI: 10.1039/c3cc47480a

www.rsc.org/chemcomm

Z. Schnepp,*[ab] M. J. Hollamby,[ac] M. Tanaka,[d] Y. Matsushita,[e] Y. Xu[e] and Y. Sakka[e]

This paper describes a powerful and versatile approach that combines the benefits of sol–gel processing with controlled phase separation to yield oxide–carbide–carbon or oxide–nitride–carbon nanocomposites.

Transition metal carbides and nitrides are valuable materials for applications such as fuel cell electrocatalysis,[1] ammonia synthesis[2] and photocatalytic water splitting.[3] In these systems, the properties often depend on control of particle size, morphology and accessible surface area.[4] Sol–gel,[5] solvothermal[6] and templating[7] processes have all been used to generate carbides and nitrides with small particle size or porosity. A major hurdle that remains is the controlled and tunable synthesis of composites, particularly carbides or nitrides combined with metal oxides.[8] Such architectures are critical for applications such as noble metal-replacement in solar water splitting.[9]

Combining two different ceramics in a nanocomposite presents a significant synthetic challenge. Historically, it has been achieved simply by mechanical mixing, which can seriously compromise the properties of one or both components. More effective methods use ammonolysis[10,11] or temperature programmed reduction[12] of oxide–oxide nanocomposites but have the disadvantage of using hazardous synthesis gases, or multi-step processes. Pinpointing more efficient and sustainable synthesis routes is critical to future materials design.[13] On this basis, a generalised one-pot sol–gel method to composites of two or more ceramic materials would have the key advantages of: (i) a single heating step, (ii) fine-tuning of particle size while achieving good interspersion and (iii) standard, inexpensive and non-hazardous synthesis atmospheres such as nitrogen.

Recently, we have shown that abundant biopolymers such as alginate are effective precursors for synthesis of oxide,[14] nitride[15] or carbide[16] nanostructures. Biopolymers are particularly suited to control of particle size in ceramics due to their ability to bind strongly to metal cations.[17] Remarkably, it is also possible to force oxide/carbide or oxide/nitride phase separation from these homogeneous precursors by exploiting differences in stability of intermediate oxides.[18] So far, however, full separation was only achieved in one system (Fe_3C–MgO).[19] In this paper, we demonstrate the versatility of the sol–gel route in the synthesis of a family of nanocomposites. This new general route emphasizes the potential of sol–gel methods for synthesis of multifunctional materials.

Nanocomposites of TiO_2–Fe_3C, TiO_2–WN, CeO_2–Fe_3C, CeO_2–WN, MgO–Fe_3C and MgO–WN were synthesized by mixing aqueous (or ethanolic) metal salts with hot gelatin solution, stirring vigorously and then drying at 80 °C. The resulting sponge-like precursors were calcined under nitrogen. Samples are denoted TF, TW, CF, CW, MF and MW. A range of molar ratios (100 : 0, 75 : 25, 50 : 50 and 0 : 100) were prepared for each sample and labelled 0, 25, 50 and 100 respectively. For example, sample TF25 was prepared with 75 mol% of Ti and 25 mol% Fe. Full sample details are listed in Table S5 (ESI†). The extent of foaming depended on the nature of the metal precursors and a higher amount of nitrate led to increased foaming, suggesting that foaming resulted from nitrate-oxidation of the polymer. Scanning electron microscopy (SEM) images show that the open, sponge-like structure is maintained even after calcination, as observed previously (Fig. S1, ESI†).[19]

Synchrotron X-ray diffraction (SXRD) patterns (Fig. 1, Fig. S2–S7, ESI†) reveal two distinct crystalline phases in each sample: an oxide (MgO, TiO_2 or CeO_2) combined with either Fe_3C or WN. The broad peaks suggest very small crystallites, which could indicate that intermixing of two crystalline phases restricts sintering compared to the sol–gel synthesis of a single phase. There is no evidence for ternary phases (*e.g.* $FeTiO_3$) and negligible peak shifting (Fig. S8 and S9, ESI†). This suggests a high level of phase separation, and phase pure carbide or nitride phases, which is in stark contrast with our first report

[a] *International Center for Young Scientists, National Institute for Materials Science (NIMS), Tsukuba, Japan*
[b] *School of Chemistry, University of Birmingham, UK. E-mail: z.schnepp@bham.ac.uk*
[c] *University of Keele, Keele, UK*
[d] *Synchrotron X-ray Station at SPring-8, NIMS, Hyogo, Japan*
[e] *National Institute for Materials Science, Tsukuba, Japan*

† Electronic supplementary information (ESI) available: Full experimental details and extra figures. See DOI: 10.1039/c3cc47480a

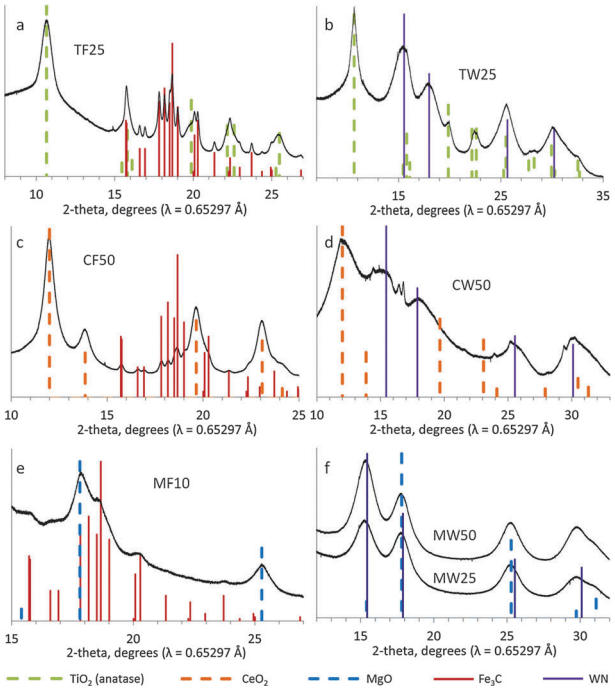

Fig. 1 Synchrotron X-ray diffraction (SXRD) patterns for (a) TiO_2/Fe_3C, (b) TiO_2/WN, (c) CeO_2/Fe_3C, (d) CeO_2/WN, (e) MgO/Fe_3C and (f) MgO/WN. The additional sharp peaks in CW50 correspond to minor W and WC phases.

of sol–gel synthesis of oxide–nitride mixtures using Ti and W (Fig. S10, ESI†).[18]

Transmission electron microscopy (TEM) images show nanoparticles interspersed in a carbon matrix (Fig. 2a and Fig. S11, ESI†). High-res TEM images of all samples show individual single crystals that can be assigned to oxide, nitride or carbide phases (Fig. 2b and Fig. S11, ESI†). In all cases, the phases are highly interspersed, supported by elemental mapping and energy dispersive X-ray analysis (EDXA) of a sample of TiO_2/Fe_3C (Fig. 2c–e). The Fe_3C particles are larger (~20 nm) than the oxide or WN particles (~2–5 nm). This is consistent with the very broad SXRD peaks for WN and the oxides, compared to the sharper peaks for Fe_3C. The Fe_3C particles are also characterized by 'onion-like' layers of graphite (Fig. S12, ESI†). This is a common observation in the synthesis of Fe_3C due to catalytic graphitization.[20] Given that Fe_3C-catalyzed graphitization is known to occur alongside (and perhaps as a result of) Fe_3C melting,[21] the agglomeration of molten Fe_3C droplets could explain the larger particle size. It should be noted that the Fe_3C particle size in these systems is still much smaller than in the sol–gel synthesis of single-phase Fe_3C from gelatin.[16] The flexible nature of this method is demonstrated in the synthesis of TiO_2/Fe_3N (Fig. S13, ESI†). Forming the nitride phase rather than the carbide Fe_3C was achieved simply by reducing the organic/metal ratio and lowering the heating temperature to 700 °C. The control of nitride *vs.* carbide formation has been observed in single-phase systems[22] and is thought to be due to stabilization of a metastable nitride phase.[15]

A study of the formation of TiO_2–Fe_3C has offered some surprising new insights into the mechanism. Many combinations of elements form stable ternary oxides, some of which are naturally occurring minerals *e.g.* ilmenite ($FeTiO_3$) or magnesioferrite ($MgFe_2O_4$). It could therefore be expected that heating a homogeneous mixture of *e.g.* Fe:Ti would initially form a ternary Fe–Ti–O phase. Indeed, there are several reports of sol–gel synthesis of Fe–Ti–O ternary compounds.[23,24] However, SXRD samples quenched at 100 °C intervals (Fig. S14, ESI†) did not show any ternary phases. Given the broad peaks, it is difficult to identify any crystalline phases other than anatase and a small amount of Fe_3N (a metastable precursor to Fe_3C).[25] However, when comparing SXRD patterns for samples TF50 and TF25 at 600 °C (Fig. 3a), very broad peaks of magnetite can be observed for TF50. Furthermore, HRTEM images (Fig. 3b) clearly show crystallites of magnetite, and STEM (inset) shows distinct Fe and Ti regions. Magnetite has been identified as an intermediate in the sol–gel synthesis of pure Fe_3C,[15] but it is surprising that it exists in this mixed system.

As a proof of concept, the MgO/Fe_3C/C sponges were tested in catalytic methanol decomposition ($CH_3OH \rightarrow 2H_2 + CO$). Methanol is of interest as a 'hydrogen carrier': storing H_2 in a safer and more manageable form.[26] The MgO–Fe_3C system was chosen because of the previous high activity of this system in the oxygen reduction reaction (ORR).[19] Also, iron carbides are

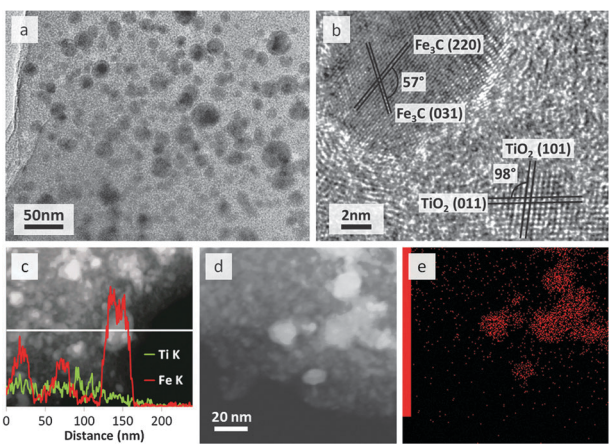

Fig. 2 (a) TEM (b) high resolution TEM, (c) EDXA line scan, (d) dark field STEM and (e) corresponding elemental map for sample TiO_2/Fe_3C.

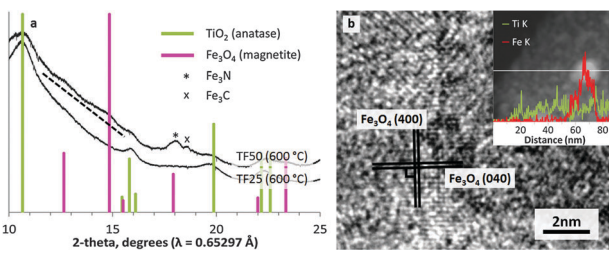

Fig. 3 (a) PXRD patterns for samples with Ti : Fe molar ratios of 50 : 50 and 75 : 25 (denoted TF50 and TF25 respectively), quenched at 600 °C during heating under N_2 (*NB*: dashed line added to highlight broad magnetite peaks). (b) High-res TEM and (inset) STEM-EDXA line analysis of sample TF50 quenched at 600 °C.

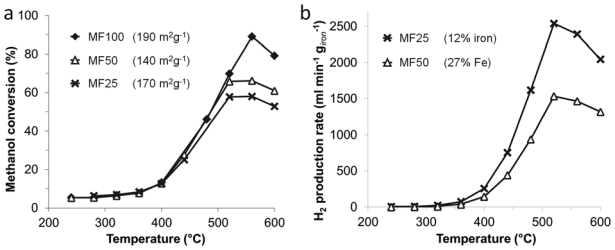

Fig. 4 (a) Percentage methanol conversion with increasing temperature for samples prepared using Mg : Fe molar ratios of 75 : 25, 50 : 50 and 0 : 100, denoted MF25, MF50 and MF100 respectively (inset BET surface areas). (b) H_2 production rate per gram of iron for MF25 and MF50 (calculated from elemental analysis).

promising materials for many other catalytic processes such as Fischer–Tropsch[27] and the ORR.[28] Fig. 4 shows the temperature dependent activity for samples MF50 and MF25 (50 and 25 mol% Fe respectively) compared to a control (100 mol% Fe) sample labelled MF100. These data show an onset of decomposition of $\sim$300 °C followed by a sharp rise up to 520 °C. After this point, the activity drops due to carbon build-up poisoning the catalyst. This deposition of carbon onto iron-containing catalysts (and some other transition metal compounds) is common in catalytic reactions involving carbon-rich gases.[29] Significantly, before the catalysts are deactivated, the activity of all three is very similar. This is surprising given that the samples contain very different amounts of Fe. The total surface area (Fig. 4a) is similar for all samples, implying that active surface area is the key factor. This can be clearly seen in a plot of H_2 production rate per gram of iron (calculated from elemental analysis). In this case, the activity of sample MF25 is much higher than that of MF50, indicating that the active surface area in MF25 is higher. This is consistent with the much smaller Fe_3C particle size in MF25, as observed by TEM and SAXS,[19] which is a result of the higher amount of MgO reducing sintering of Fe_3C. Selectivity is high (Fig. S15–S17, ESI†) and the H_2/CO ratio stabilizes at 2 (Fig. S18, ESI†). The high initial H_2/CO ratio could indicate side reactions such as $2CO_{(g)} \rightleftharpoons C_{(s)} + CO_{2(g)}$. Carbon balances (Tables S1–S3, ESI†) give very small variation (<5%).

The activity of this Fe_3C/MgO catalyst for methanol decomposition is lower than for optimized catalysts.[30,31] However, this is a compelling demonstration of improved mass-activity through optimizing particle size and dispersion. The data offer a good starting point for investigation of oxide/carbide and oxide/nitride materials as catalysts. This field has recently attracted a lot of attention[32] and the simple, sol–gel preparation of carbide or nitride composites with metal oxides offers a cost-effective and sustainable alternative to existing multi-step routes. Furthermore, there are many simple ways to optimize the sol–gel synthesis (*e.g.* biopolymer type, or drying rate).

In summary, we have demonstrated a flexible and general method for producing composites of transition metal nitrides or carbides with metal oxides. The homogeneous sol–gel precursor and simultaneous evolution of two distinct crystalline phases minimizes the particle size (<20 nm). Furthermore the two phases are highly interspersed, which offers high *active* surface areas, as demonstrated by enhanced catalytic activity per gram. This simple and robust and flexible method therefore offers considerable advantages over previous multi-step methods for generating oxide–carbide and oxide–nitride composites.

The authors thank NIMS-ICYS, JSPS, SPring-8 (2012A4511) and University of Birmingham.

Notes and references

1 Z. Wen, S. Ci, F. Zhang, X. Feng, S. Cui, S. Mao, S. Luo, Z. He and J. Chen, *Adv. Mater.*, 2012, **24**, 1399–1404.
2 A.-M. Alexander and J. S. J. Hargreaves, *Chem. Soc. Rev.*, 2010, **39**, 4388–4401.
3 A. T. Garcia-Esparza, D. Cha, Y. Ou, J. Kubota, K. Domen and K. Takanabe, *ChemSusChem*, 2013, **6**, 168–181.
4 L. Borchardt, C. Hoffmann, M. Oschatz, L. Mammitzsch, U. Petasch, M. Hermann and S. Kaskel, *Chem. Soc. Rev.*, 2012, **41**, 5053–5067.
5 Y. Kido, K. Nakanishi, A. Miyasaka and K. Kanamori, *Chem. Mater.*, 2012, **24**, 2071–2077.
6 B. Mazumder and A. L. Hector, *J. Mater. Chem.*, 2008, **18**, 1392–1398.
7 Y. Shi, Y. Wan and D. Zhao, *Chem. Soc. Rev.*, 2011, **40**, 3854–3878.
8 M. Feyen, C. Weidenthaler, R. Güttel, K. Schlichte, U. Holle, A.-H. Lu and F. Schüth, *Chem.–Eur. J.*, 2011, **17**, 598–605.
9 Y. Kim, H. Irie and K. Hashimoto, *Appl. Phys. Lett.*, 2008, **92**, 182107.
10 N. Liu, L. Nie, N. Xue, H. Dong, L. Peng, X. Guo and W. Ding, *ChemCatChem*, 2010, **2**, 167–174.
11 P. Krawiec and S. Kaskel, *Top. Catal.*, 2009, **52**, 1549–1558.
12 D.-V. N. Vo and A. A. Adesina, *Appl. Catal., A*, 2011, **399**, 221–232.
13 *A Sustainable Global Society (White paper)*, Royal Society of Chemistry, 2011.
14 Z. Schnepp, S. R. Hall, M. J. Hollamby and S. Mann, *Green Chem.*, 2011, **13**, 272–275.
15 Z. Schnepp, M. Thomas, S. Glatzel, K. Schlichte, R. Palkovits and C. Giordano, *J. Mater. Chem.*, 2011, **21**, 17760–17764.
16 Z. Schnepp, S. C. Wimbush, C. Giordano and M. Antonietti, *Chem. Mater.*, 2010, **22**, 5340–5344.
17 Z. Schnepp, *Angew. Chem., Int. Ed.*, 2013, **52**, 1096–1108.
18 Z. Schnepp, M. J. Hollamby, M. Tanaka, Y. Matsushita, Y. Katsuya and Y. Sakka, *Sci. Tech. Adv. Mater.*, 2012, **13**, 035001.
19 Z. Schnepp, Y. Zhang, M. J. Hollamby, B. R. Pauw, M. Tanaka, Y. Matsushita and Y. Sakka, *J. Mater. Chem. A*, 2013, **1**, 13576–13581.
20 Y. Homma, Y. Kobayashi, T. Ogino, D. Takagi, R. Ito, Y. J. Jung and P. M. Ajayan, *J. Phys. Chem. A*, 2003, **107**, 12161–12164.
21 S. Glatzel, Z. Schnepp and C. Giordano, *Angew. Chem., Int. Ed.*, 2013, **52**, 2355–2358.
22 C. Giordano, C. Erpen, W. Yao and M. Antonietti, *Nano Lett.*, 2008, **8**, 4659–4663.
23 X. Tang and K. Hu, *J. Mater. Sci.*, 2006, **41**, 8025–8028.
24 Y. G. Sharma, M. Kharkwal, S. Uma and R. Nagarajan, *Polyhedron*, 2009, **28**, 579–585.
25 K. H. Jack, *Proc. R. Soc. London, Ser. A*, 1948, **195**, 34–40.
26 S. Sá, H. Silva, L. Brandão, J. M. Sousa and A. Mendes, *Appl. Catal., B*, 2010, **99**, 43–57.
27 E. De Smit and B. M. Weckhuysen, *Chem. Soc. Rev.*, 2008, **37**, 2758–2781.
28 Z. Wen, S. Ci, F. Zhang, X. Feng, S. Cui, S. Mao, S. Luo, Z. He and J. Chen, *Adv. Mater.*, 2012, **24**, 1399–1404.
29 C. H. Bartholomew, *Catal. Rev. Sci. Eng.*, 1982, **24**, 67–112.
30 G. Marbán, A. López, I. López and T. Valdés-Solís, *Appl. Catal., B*, 2010, **99**, 257–264.
31 J. H. Jang, Y. Xu, M. Demura, D. M. Wee and T. Hirano, *Appl. Catal., A*, 2011, **398**, 161–167.
32 J. S. J. Hargreaves, *Coord. Chem. Rev.*, 2013, **257**, 2015–2031.

